2016

Plasma Density Analysis of CubeSat Wakes in the Earth's Ionosphere

Robert M. Albarran II

Aroh Barjatya
Embry-Riddle Aeronautical University, barjatya@erau.edu

Scholarly Commons Citation

Albarran, R. M., & Barjatya, A. (2016). Plasma Density Analysis of CubeSat Wakes in the Earth's Ionosphere. *Journal of Spacecraft and Rockets, 53*(3). https://doi.org/10.2514/1.A33402

JOURNAL OF SPACECRAFT AND ROCKETS
Vol. 53, No. 3, May-June 2016

Plasma Density Analysis of CubeSat Wakes in the Earth's Ionosphere

Robert M. Albarran, II* and Aroh Barjatya†
Embry–Riddle Aeronautical University, Daytona Beach, Florida 32114

DOI: 10.2514/1.A33402

Spinning or tumbling CubeSats with Langmuir probes deployed on booms will render spin-modulated plasma densities as the probes move in and out of the spacecraft wake. It is traditionally assumed that the lower-density measurements from the spin cycle are made in the spacecraft wake, and the higher-density measurements are outside the wake. Although this assumption is valid for larger spacecraft in the Earth's ionosphere, this paper scrutinizes its validity for CubeSats in similar conditions. Spacecraft–plasma interactions (surface charging, plasma sheaths, and wakes) are less understood for CubeSats, and the small CubeSat dimensions must be considered with respect to characteristic length scales of the space plasma environment, namely, the Debye length. Spacecraft Plasma Interaction Software, a spacecraft charging analysis tool, is used to investigate CubeSat interactions with the mesothermal plasma environment. For low-density and cold-plasma ionospheric conditions, the CubeSat dimension of 10 cm is comparable to the sheath thickness. The simulations show that, under such circumstances, a negatively charged CubeSat in mesothermal ionospheric conditions creates an ion focus region in the far wake. An independently written, first-principles code in MATLAB demonstrates that this feature is a direct result of the CubeSat behaving like a Langmuir probe in the thick-sheath model. The work performed in this paper cautions the community toward assuming CubeSats to have density depletion in their wake and stresses the necessity of having an accurate attitude solution and proper boom length design to derive ambient plasma densities from spin-modulated Langmuir probe measurements on CubeSats.

Nomenclature

A	=	surface area, m^{-2}
$\boldsymbol{a}$	=	ion acceleration vector, $m \cdot s^{-2}$
I_e	=	electron current, A
I_i	=	ion current, A
ℓ	=	dimension of conductor, m
n_e	=	electron density, m^{-3}
n_i	=	ion density, m^{-3}
n_0	=	quasi-neutral plasma density, m^{-3}
$\boldsymbol{r}_i$	=	ion position vector, m
T_e	=	electron temperature, K
T_i	=	ion temperature, K
$\boldsymbol{v}_{\mathrm{SC}}$	=	spacecraft velocity vector, $m \cdot s^{-1}$
$\boldsymbol{v}_i$	=	ion velocity vector, $m \cdot s^{-1}$
$\boldsymbol{v}_{\mathrm{the}}$	=	electron thermal velocity vector, $m \cdot s^{-1}$
$\boldsymbol{v}_{\mathrm{thi}}$	=	ion thermal velocity vector, $m \cdot s^{-1}$
λ_D	=	Debye length, m
τ_C	=	charging time, s
ϕ_f	=	floating potential, V
ϕ_p	=	plasma potential, V
ϕ_s	=	sheath potential, V
χ	=	ion focusing parameter, m
ω_p	=	plasma frequency, $rad \cdot s^{-1}$

I. Introduction

LANGMUIR probes are the most routinely used plasma diagnostic instruments aboard satellites and sounding rockets [1,2]. Spacecraft typically deploy Langmuir probes on booms into the space plasma environment and apply electrostatic probe theory as developed by Irving Langmuir [3] and Mott-Smith and Langmuir [4] in the mid-1920s for data analysis. With the widespread acceptance of the CubeSat specification for small satellites [5], Langmuir probes are being deployed on multiple CubeSats [6]. Because Langmuir probes are among the most simple instruments that offer in situ plasma diagnostic measurements, their inclusion in a future CubeSat constellation is imminent. As a result, spacecraft–plasma interactions of a CubeSat (charging, sheaths, and wakes) must be studied to properly design Langmuir probes and analyze the acquired measurements.

High relative velocity of an object traveling with respect to the plasma generates a plasma wake [7]. Particle-in-cell (PIC) codes track the trajectories of charged particles in a Lagrangian reference frame in phase space with respect to a background Eulerian coordinate system in response to self-consistent electrodynamic or electrostatic fields. PIC codes are commonly employed to simulate plasma wakes for various conditions [8–11]. In general, plasma wakes have been seen to be generated by various objects in the space plasma environment: from high-velocity dust grains [8,12,13] to spacecraft [14–16] and planetary bodies [9,17–20].

In the absence of spurious currents (photoemission, backscattered and secondary electrons, electron beams, etc.), spacecraft surfaces in the ionosphere tend to charge to negative potentials. Furthermore, the Earth's ionosphere is typically a mesothermal environment for satellites such that $\boldsymbol{v}_{\mathrm{the}} \gg \boldsymbol{v}_{\mathrm{SC}} \gg \boldsymbol{v}_{\mathrm{thi}}$, where $\boldsymbol{v}_{\mathrm{the}}$, $\boldsymbol{v}_{\mathrm{SC}}$, and $\boldsymbol{v}_{\mathrm{thi}}$ are electron thermal velocity, spacecraft velocity, and ion thermal velocity, respectively. The thermal velocity for the s-species particle of temperature T_s and mass m_s is taken here as the most-probable thermal velocity of the form $v_{\mathrm{ths}} = (2k_B T_s/m_s)^{1/2}$, where k_B is the Boltzmann constant. Positively charged ions are subsonic with respect to the bulk flow velocity such that they contribute to the ram-side flux current [7]. This generally results in an ion density depletion in the wake of spacecraft. Consequently, density measurements from Langmuir probes differ when taken within or outside a plasma wake; an asymmetry in the wake current distribution has been shown to exist [21]. For spin-modulated Langmuir probe measurements, it is assumed that the lesser density at any given time corresponds to the probe being in the wake, whereas the greater density is thought to be given by the probe outside the wake. Furthermore, it has been numerically verified that positively charged ion trajectories may be modulated in the presence of a negatively charged object giving rise

Received 2 August 2015; revision received 10 November 2015; accepted for publication 14 November 2015; published online 28 April 2016.

*Ph.D. Candidate, Engineering Physics, Department of Physical Sciences, 600 South Clyde Morris Boulevard.

†Associate Professor, Engineering Physics, Department of Physical Sciences, 600 South Clyde Morris Boulevard.

to an ion density enhancement in the wake [11,22]. Heavy ions contribute to the geometric wake structure, whereas the negatively charged conductor acts as an electrostatic lens for light ions [23]. The region of light ion focusing is typically referred to as the ion focus region [17].

The ion focus region is dependent on the geometry of the negatively charged body; a degree of asymmetry in focusing is present for elongated objects [24]. Density enhancements in the focus region are more prevalent for cold ions because they lack the energy to escape electrostatic lensing [11]. The maxima of density enhancement in the ion focus region resides farther downstream for high-velocity objects [23]. Moreover, a potential maximum follows the density enhancement downstream as given by Poisson's equation [25]. The ion focus region has been studied for electrically charged dust grains [12,13], non-CubeSat spacecraft [23], and planetary bodies [9,18]. Nevertheless, previous studies of plasma wakes have not discovered ion focusing for the CubeSat form factor [26,27].

In this paper, the open-source PIC code Spacecraft Plasma Interaction Software (SPIS) is used to model the plasma wake of a CubeSat with densities that are typical of nighttime, midlatitude, topside ionospheric environment where the local Debye length is comparable to the CubeSat dimension. SPIS has been successfully employed in the past to model spacecraft–plasma interactions [28–30]. For simplicity, zero background magnetic field is assumed. The ion enhancement in the far wake rendered by SPIS is validated by a first-principles code in MATLAB. The ion focus region has profound implications on Langmuir probe design and data analysis for CubeSats.

II. CubeSat Surface Charging

A negatively charged conducting surface results in a departure from quasi neutrality in the local ambient plasma; a net electron deficit occurs in the immediate vicinity of the surface, generating an ion dominant region of negative plasma potential [31]. For a Debye length λ_D, plasma potential ϕ_p, electron density n_e, and ion density n_i, $n_e < n_i$ ($\phi_p < 0$) within the Debye sheath of thickness $n\lambda_D$, where $n \sim 5-7$. Outside the Debye sheath, plasma attains quasi neutrality, that is, $n_e = n_i = n_0$ and $\phi_p = 0$. The electron and ion density profile as a function of distance from a charged surface is illustrated in Fig. 1 [32].

In general, the electrostatic influence of a charged conductor on the angular momentum of charged particles dominates when the dimension of the conductor, ℓ, is less than or comparable to the sheath thickness, that is, $n\lambda_D \geq \ell$. This type of interaction is characterized by orbital-motion-limited theory and constitutes the thick-sheath model. Alternatively, when $\ell \geq n\lambda_D$, particle angular momentum is relatively unchanged in what constitutes the space charge regime or thin-sheath model [33].

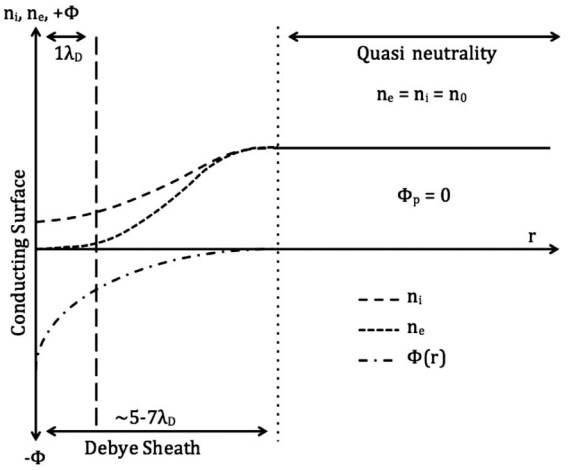

Fig. 1 The sheath extends $n\lambda_D$ (for $n \sim 5-7$) from the negatively charged conducting surface. Beyond $n\lambda_D$, quasi neutrality holds and $\phi_p = 0$ (not to scale). Adapted from [32].

Table 1 CubeSat charging times and floating potentials for topside-ionospheric conditions

Simulation	n_0, m^{-3}	$T_e = T_i$, K	τ_C, s	ϕ_f, V
1	1×10^9	1000	6.22×10^{-5}	−0.30
2	1×10^9	2000	9.28×10^{-5}	−0.59
3	1×10^9	3000	1.19×10^{-4}	−0.87
4	1×10^8	1000	4.70×10^{-4}	−0.27
5	1×10^8	2000	1.10×10^{-3}	−0.58
6	1×10^8	3000	2.10×10^{-3}	−0.90

Just as Langmuir probe surface currents are determined by applied bias potentials, the potential of a spacecraft is a response from accumulated surface currents [7]. In this manner, CubeSats in the Earth's ionosphere behave as Langmuir probes in the thick-sheath regime, that is, $\ell \approx n\lambda_D$ for typical topside ionospheric values of $\lambda_D \approx 3$ cm and $\ell \approx 10$ cm. In the absence of photoemission, CubeSats charge negatively to low potentials in mesothermal topside ionospheric conditions. We use the nonlinear Poisson solver in the SPIS numerical kernel (SPIS-NUM) with an O^+ ion population simulated as particle-in-cell in electrostatic balance with a Maxwellian electron velocity distribution function. The nonlinearity occurs from the electron distribution function tending toward thermodynamic equilibrium by stochastic collisions with the O^+ population. Particle dynamics on these time scales are guaranteed to be captured in the simulation because a 1×10^{-6} s plasma time step is selected to be on the order of the local plasma frequency inverse [28]. The time step selected is much less than the ion acoustic frequency inverse such that all PIC ion dynamics are resolved on these time scales.

Within the SPIS simulation, the time it takes for the PIC simulation to converge to a floating potential ϕ_f corresponding to zero net surface current, τ_C, is considered. The values of τ_C and ϕ_f for two different densities ($n_0 = 1 \times 10^9$ m^{-3} and $n_0 = 1 \times 10^8$ m^{-3}) and three different temperatures (1000, 2000, and 3000 K) are tabulated in Table 1. For a stationary CubeSat, charged particles accumulate on surfaces by purely thermal motion. As expected, Table 1 and Fig. 2 show that ϕ_f is independent of plasma density and only dependent on plasma temperature. The figures and the table also show that $\tau_C \propto (T_e, T_i)$ and $\tau_C \propto n_0^{-1}$. Note that τ_C is not the same as the time it takes for a simulation to run. With a 1 s : 100 min PIC-to-real-time ratio, for $t \geq \tau_C$ the plasma potential field is steady-state. For the simulation time steps and plasma volume size considered, more particles than $n_0 = 1 \times 10^{10}$ m^{-3} exceeded the processing power for the large computational domain in SPIS.

III. Simulation Parameterization

To remain within reasonable computational expense of SPIS-NUM in the thick-sheath approximation of Langmuir probe theory, we simulate a space plasma environment that is absent of energetic particles, spurious surface currents, and magnetic fields. The plasma densities chosen are representative of midlatitude, nighttime, geomagnetically quiet, topside (greater than 400 km) ionospheric regions or, equivalently, low-density plasma bubbles, where the Debye sheath is comparable or larger than the CubeSat size. Thus, we simulate a single-electrical-node 1.5U CubeSat traveling at 7.5 km $\cdot$ s^{-1} immersed in a quasi-neutral plasma density of $n_0 = 8 \times 10^9$ m^{-3} in SPIS. The electron (ion) temperature is $T_e =$ 2000 K ($T_i = 1400$ K) such that the local Debye length is $\lambda_D = 3.5 \times 10^{-2}$ m. The local plasma frequency is $\omega_p = 5 \times 10^6$ rad $\cdot$ s^{-1}. A 0.75 m ($\approx 21.5\lambda_D$) radius spherical computational volume accommodates the 1.5U CubeSat with the 15 cm dimension along the velocity vector (the x axis) at zero ram angle. The CubeSat is offset from the center of the computational domain by 30 cm toward the ram direction with ions flowing with velocity $\boldsymbol{v} = \boldsymbol{v}_{SC}\hat{e}_x$ for $\boldsymbol{v}_{SC} \gg \boldsymbol{v}_{thi}$ and $\boldsymbol{v}_{SC} = 7500$ m $\cdot$ s^{-1}. The geometry designed in Gmsh is illustrated in Fig. 3.

The spacecraft surface is modeled as an aluminum cuboid with 300 K surface temperature. Realistically, only the rails of the CubeSat constitute the conducting area. As a result, as long as the Debye length is comparable or larger to the dimensions of the CubeSat, the

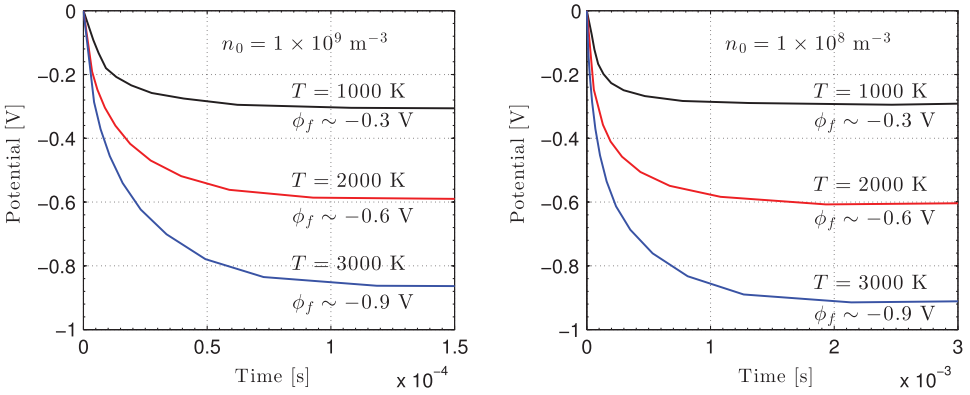

Fig. 2 CubeSat floating potentials for an O^+ dominant plasma environment.

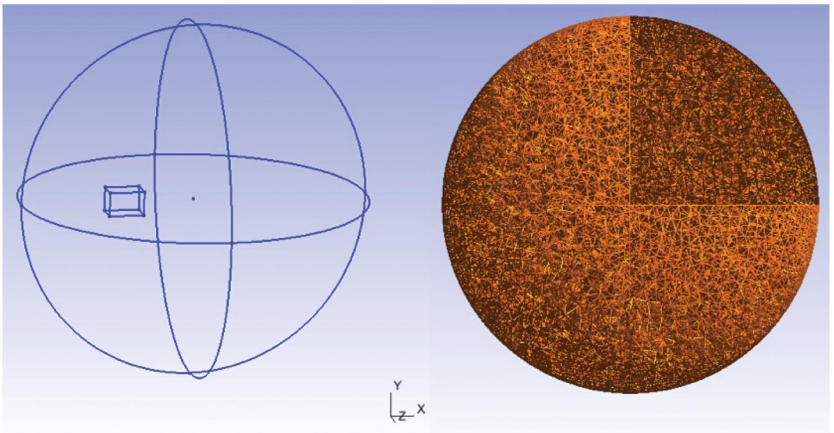

Fig. 3 The 1.5U CubeSat within a spherical computational volume of 0.75 m radius. No external appendages are modeled.

effect of only the rails being charged is similar to the CubeSat being approximated as a solid cuboid. In this investigation, we have not studied the effect of a biased Langmuir probe extended on a boom. Note that, while using Langmuir probes, one always designs the probe to be such that the measurement itself does not disturb the environment that needs to be measured. Furthermore, when one is doing Langmuir probe analysis, one again assumes that the measurement from the probe is representative of the environment and that the environment is not being disturbed by the probe presence itself. Thus, we have only concentrated on the effect that the presence of the spacecraft has on the surrounding plasma environment.

Surface currents are computed for a specified particle distribution function: bi-Maxwellian, Maxwellian, backtracking, or particle-in-cell (PIC). Spacecraft surface and plasma sheath potentials are, likewise, derived by electrodynamic boundary conditions. Thermal motion toward thermodynamic equilibrium in the spacecraft vicinity is itself nonlinear. With a PIC modeled O^+ ion population and given quasi-neutral density, the nonlinear Poisson solver of SPIS-NUM obtains a plasma potential field by the common preconditioned conjugate gradient algorithm. Particle accelerations coherent to the potential field are thus consistent with collisional effects, ambipolar diffusion, and other magnetohydrodynamic phenomena. Plasma field densities are interpolated in SPIS-NUM from particle positions that result from integrating particle accelerations by the leap-frog scheme.

Because of simulated mesothermal conditions, the CubeSat ram surface area is subject to a flux of PIC-modeled O^+ ions with $\boldsymbol{v}_{\text{thi}} \ll \boldsymbol{v}_{\text{SC}}$. Differential surface charging is nonexistent for an electrically connected structure. Because the spacecraft is subsonic with respect to electrons, that is, $\boldsymbol{v}_{\text{SC}} \ll \boldsymbol{v}_{\text{the}}$, the CubeSat is subject to an isotropic thermal flux of Maxwellian electrons. Background magnetic fields are not considered, and spacecraft charge neutralization omits the inclusion of induced magnetic fields after τ_C. Pertinent plasma and simulation global parameters are referenced in Table 2.

IV. Simulation Results of CubeSat–Plasma Interactions

The Maxwellian electron population is isotropically repelled from the negatively charged CubeSat surface in the exponential fashion of the Boltzmann repulsion factor. The CubeSat floats to $\phi_f \approx -0.67$ V at $\tau_C \approx 5.20 \times 10^{-5}$ s, as seen in Fig. 4. The time of charging onset τ_C is defined as the time of minimum absolute net current I_T. Here, as time approaches $\tau_C \approx 5.20 \times 10^{-5}$ s, the surface current is neutralized, and the spacecraft potential ϕ approaches the floating potential of $\phi_f \approx -0.67$ V, that is, $I_T \to 0$ and $\phi \to \phi_f$ for $t \to \tau_C$. However, for $0 < t < \tau_C$, when the simulation has not converged to the final bias point, the thermal electron collection current is larger than the thermal ion collection current. Thus, the net current collection is initially negative. For $t \geq \tau_C$ and $\boldsymbol{v}_{\text{SC}} \gg \boldsymbol{v}_{\text{thi}}$, the sheath potential and thickness are modulated according to ambipolar diffusion of Maxwellian electrons in response to the nonsymmetric ion density distribution in the ram and wake sides until surface currents are neutralized by attracted ions. Constant surface charge neutralization causes continuous yet minor (less than 10%)

Table 2 SPIS-NUM simulation parameters for a single-electric-node 1.5 U CubeSat geometry

Parameter	Value
Electron volume distribution	Global Maxwell–Boltzmann
Ion volume distribution	PIC
Electron density n_e	8×10^9 m^{-3}
Ion density n_i	8×10^9 m^{-3}
Electron temperature T_e	2000 K
Ion temperature T_i	1400 K
Plasma Dt	1×10^{-6} s
Simulation duration τ_C	2×10^{-4} s
CubeSat ram velocity $\boldsymbol{v}_{\text{SC}}$	7500 m · s^{-1}

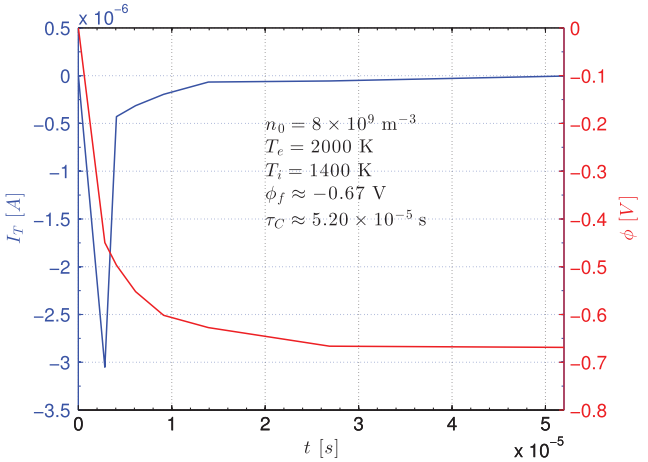

Fig. 4 CubeSat net surface current I_T and potential ϕ as a function of time.

fluctuations in spacecraft floating potential and ambient plasma density even after the spacecraft reaches the floating potential ϕ_f.

The triangulation of $\boldsymbol{v}_{\text{thi}}$ and $\boldsymbol{v}_{\text{SC}}$ at a distance $n\lambda_D$ downstream along the wake axis creates a Mach cone with an ion density depletion in the near wake, as seen in Fig. 5. The simulation also shows an enhanced ion density region in the far wake. This is a direct effect of electrostatic lensing of the ion that did not impact the ram surface but got influenced by the negative potential of the CubeSat surface.

Via ambipolar electric fields, an electron density enhancement also exists within the ion focus region, as well as a positive plasma potential, as shown in Figs. 6 and 7, respectively. Note that, because electron charge is negative, the left of the scale (blue) signifies higher

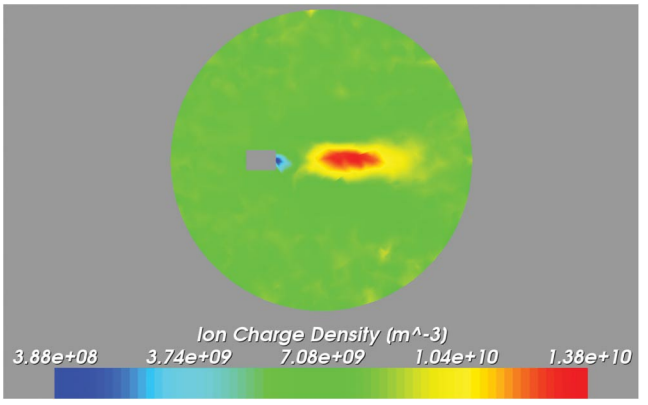

Fig. 5 Ion charge density through the principal axis along the spacecraft velocity vector.

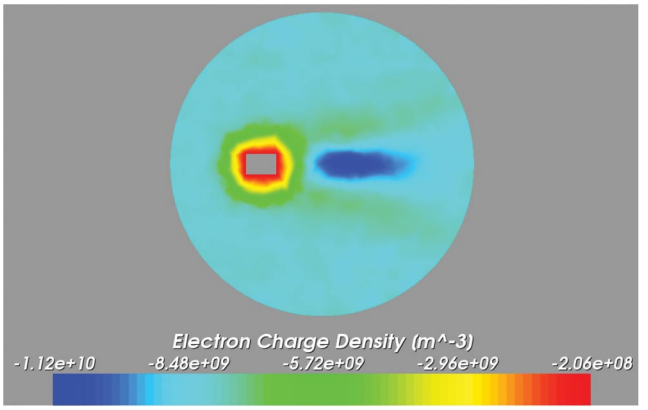

Fig. 6 Electron charge density through the principal axis along the spacecraft velocity vector.

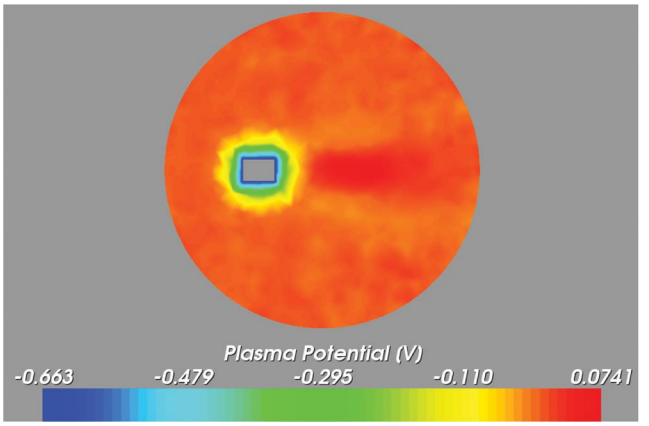

Fig. 7 Plasma potential through the principal axis along the spacecraft velocity vector.

electron density. Figure 6 also shows a bow shock in electron density. The ion density also has a bow shock but is not clear in Fig. 5 due to the linear color scale. Figure 7 demonstrates that, because the CubeSat surface is charged negative, the ambient plasma potential slowly rises to zero after several Debye lengths, just as expected in Fig. 1.

Figures 8 and 9 show the plasma parameters (n_e, n_i, and ϕ_p) along slices of the computational volume: one perpendicular to the ram direction and another parallel to the ram direction, respectively. The

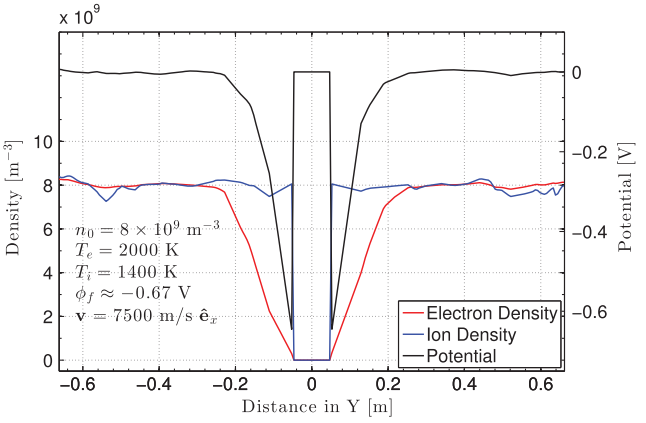

Fig. 8 Plasma density and potential profiles perpendicular to the velocity vector through the spacecraft center, $v = v_{\text{SC}}\hat{e}_x$. The Debye length is $\lambda_D = 3.5 \times 10^{-2}$ m.

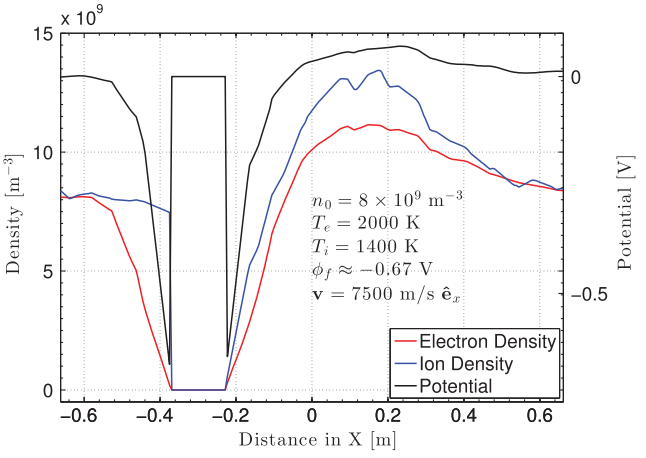

Fig. 9 Plasma density and potential profiles along the velocity vector through the spacecraft center, $v = v_{\text{SC}}\hat{e}_x$. The Debye length is $\lambda_D = 3.5 \times 10^{-2}$ m.

plasma parameter profiles in Fig. 8 are similar to a nonflowing case: electron depletion close to the negatively charged CubeSat, and an increase of the sheath potential to plasma potential as well quasi neutrality in plasma density outside the Debye sheath. On the other hand, the plasma parameter profiles in Fig. 9 show a distinct ion enhancement above the background ion density in the CubeSat wake. Because of ambipolar diffusion, this also leads to electron enhancement in the wake as well as a positive sheath potential. Massive ions do not assume diffusive equilibrium in the perturbed sheath potential on time scales comparable to the local plasma frequency inverse. As a result, the sheath potential ϕ_s is governed by the rate PIC ions respond to fluctuations in ϕ_f. The ion number densities interpolated from PIC macroparticle positions incur small (less than 10%) fluctuations at these time scales.

When Langmuir probes are deployed on booms on a spinning spacecraft, the measurable maxima is accepted as being detected outside the wake and is thus considered to be an ambient density measurement. This relies purely upon the assumption that there is always a plasma depletion in the wake, which is valid for spacecraft in the space charge regime of probe theory. The formation of an ion focus region downstream of a negatively charged conductor with dimensions comparable to the Debye sheath thickness is thus of significant concern when developing CubeSat Langmuir probes with extended booms that may lie along the velocity vector. Langmuir probes deployed on long enough booms that place it in the ion focus region will measure a plasma density enhancement over the ram-side detection and the background density.

For this particular simulation, the near wake resides within 27 cm ($\sim 7\lambda_D$) from the wake-side surface. The far wake begins 27 cm downstream and extends 88 cm ($\sim 25\lambda_D$) before the background density is recovered. The ion focus region itself extends 61 cm ($\sim 17\lambda_D$) or, equivalently, $4\ell_{||}$ ($6\ell_{\perp}$) for 1.5U CubeSat dimension parallel (perpendicular) to the direction of motion $\ell_{||} = 15$ cm ($\ell_{\perp} = 10$ cm). It is also noted that the potential maximum of $\phi \approx 0.07$ V exists in the focus region 17 cm ($\sim 5\lambda_D$) downstream the density maximum (i.e., 60.35 cm downstream the CubeSat). This is in agreement to what has previously been shown for focus regions of dust particles [25]. Ultimately, the ion focus region denotes an ion density enhancement of about 66% over n_0. Quasi neutrality is recuperated once ion trajectories are dominated by thermal velocity components toward the wake axis beyond the negatively charged near wake. The generation of the ion focus region as rendered by SPIS is central to this investigation and is independently verified to a leading approximation in the next section.

V. Confirmation of the O^+ Ion Focus Region

A first-principles two-dimensional ion-lensing code was developed in MATLAB to validate the far-wake ion density enhancements rendered by SPIS. This section confirms that the ion focus region is a result of the CubeSat operating in the thick-sheath regime where the local Debye length is comparable to the CubeSat dimensions. O^+ ion trajectories and spacecraft interactions are modeled on a per-particle basis in the spacecraft reference frame with ion velocity $\boldsymbol{v}_{\rm SC}$. For simplicity, edge effects of the CubeSat model are avoided by simulating a spherical geometry of 1.5U form factor. The spherical satellite has a radius of 9 cm and is placed at the origin. O^+ ions are released at $\boldsymbol{v}_{\rm SC}$ along the x axis with 1400 K ion thermal velocities $\boldsymbol{v}_{\rm thi}$. Although ion thermal velocities are in random directions, we only consider the two extreme cases of either directly toward or away from the principal wake axis (i.e., the x axis).

Particle motion is initiated by a bulk flow velocity $\boldsymbol{v}_{\rm SC}$ and a thermal velocity $\boldsymbol{v}_{\rm thi}$ toward the wake axis such that $\boldsymbol{v}_i = \boldsymbol{v}_{\rm SC}\hat{\boldsymbol{e}}_x \pm \boldsymbol{v}_{\rm thi}\hat{\boldsymbol{e}}_y$. Figure 10 shows the thermal wake of an uncharged spherical spacecraft, where the blue trajectories correspond to ions with thermal components away from the wake axis and red trajectories correspond to the ions with thermal components toward the wake axis. The traditional view of plasma wakes in the ionosphere has quasi neutrality for all regions outside the thermal Mach cone. The distance traveled by O^+ ions from injection to the wake axis is given by the focusing parameter χ. For an uncharged satellite, the thermal focusing parameter is

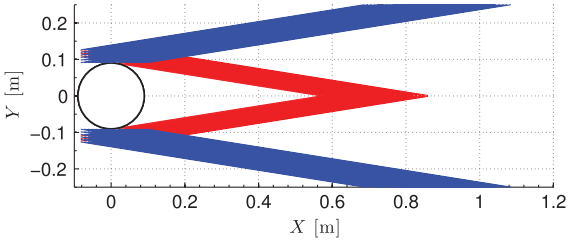

Fig. 10 Thermal plasma wake of an uncharged sphere with thermal velocities away from the wake axis (blue trajectories) and toward the wake axis (red trajectories).

$\chi_t = (\boldsymbol{v}_{\rm SC}^2 + \boldsymbol{v}_{\rm thi}^2)^{1/2}$. The conventional heavy ion geometric wake, effectively, Mach cone, of a satellite in the space charge regime of mesothermal conditions is a result of the velocity triangulation of χ_t. The wake in the absence of electrostatic interactions with the spacecraft in a mesothermal flow is effectively a thermal wake. As expected, the near-thermal wake is devoid of ions as $\boldsymbol{v}_{\rm SC} \gg \boldsymbol{v}_{\rm thi}$. For a charged spacecraft, the wake is expected to be different because the CubeSat dimensions are comparable to the Debye length. Thus, we introduce an electrostatic potential in the MATLAB model.

A plasma potential field modulates trajectories of ions for a satellite at $\phi_f \neq 0$. Ion kinematics are iteratively computed at 1 μs time steps according to the field produced by $\phi_f = -0.67$ V. With the sphere at the origin, the ion position vector is $\boldsymbol{r}_i = x\hat{\boldsymbol{e}}_x + y\hat{\boldsymbol{e}}_y$. The potential field at the ion, ϕ_p, is proportional to the e-fold decay of ϕ_f (i.e., $\phi_p \propto \phi_f e^{-r_i/\lambda_D}$) in accordance to the Debye–Hückel potential in the plasma field [34]. Figure 11 illustrates that the potential as a function of distance in the near-spacecraft environment is dominated by the exponential decay of the potential within $n\lambda_D$ of the spacecraft. The exponential contribution to the potential falls off much faster than the inverse distance term such that, in the sheath, the inverse distance term is negligible.

The electric force of the spacecraft on an ion of mass m_i and charge q_i attracts the particle toward the spacecraft antiparallel to r_i with an acceleration magnitude of

$$a = \frac{q_i}{m_i}\frac{\phi_p}{r_i} \tag{1}$$

Particle trajectories are constructed by integrating the preceding for velocities and positions. Number densities are then interpolated from the positions.

It is expected that ions within $n\lambda_D$ of the spacecraft at $\phi_f \neq 0$ will be influenced by the potential field at the ion, ϕ_p. An attractive force governed by Eq. (1) on O^+ ions of mass m_i is introduced. The wake produced by the electrostatic lensing of ion trajectories is what is

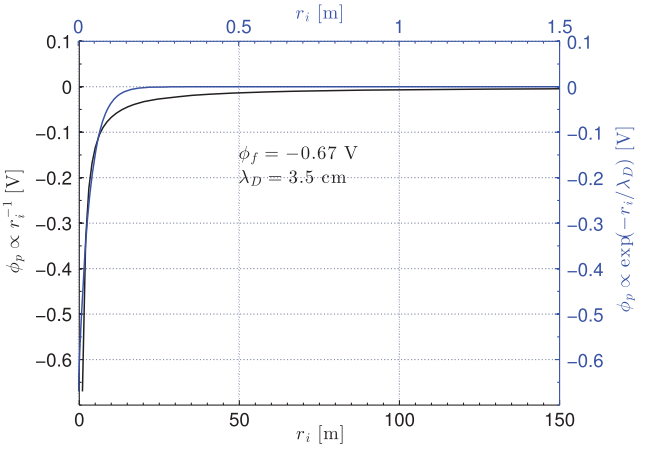

Fig. 11 Plasma potential decay rate, as measured from the skin of the satellite, is dominated by the exponential decay of $\phi_p \propto \exp(-r_i/\lambda_D)$.

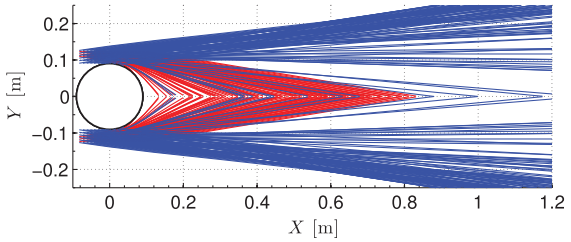

Fig. 12 Electrostatic plasma wake of a charged sphere with floating potential $\phi_f = -0.67$ V. Ion trajectories with thermal velocities toward (away) the wake axis are in red (blue).

referred to here as an electrostatic wake. The distance that ions reach the wake axis from initialization by thermal and electrostatic effects is given by the electrostatic focusing parameter χ_e. The focusing parameter for the electrostatic wake is given by the distance of the wake axis crossing from injection, $\chi_e = |x_f - x_i|$, where x_f is the final ion position along the wake axis, and x_i is the location of injection.

Figure 12 demonstrates how the negatively charged sphere focuses ions directly toward the wake axis, as symmetry suggests. Focusing applies both to ions with initial thermal velocities toward and away from the principal axis, alike. Thus, more ions reach the wake axis at distances closer to the spacecraft in the presence of $\phi_f < 0$. Attracted charges generate a density enhancement through the Mach cone and are characterized by the electrostatic focusing parameter χ_e. For the thermal wake (i.e., $\phi_f = 0$), the focusing parameter is $\chi_t = (\boldsymbol{v}_{\mathrm{SC}}^2 + \boldsymbol{v}_{\mathrm{thi}}^2)^{1/2}$, and for the electrostatic wake, $\chi_e = |x_f - x_i|$. With ion attraction, random thermal motions ensure a background thermal wake with a superposed electrostatic wake structure. For attracted species, $0 \le \chi_e \le \chi_t$. Ion thermal velocity components toward the wake axis are inversely proportional to χ, that is, $\chi \propto \boldsymbol{v}_{\mathrm{thi}}^{-1}$ for $\boldsymbol{v}_{\mathrm{thi}} \perp \boldsymbol{v}_{\mathrm{SC}}$.

Focused ions are primarily attracted from negatively charged Debye sheaths adjacent to surfaces parallel to the wake axis. The exponential decay of the sheath potential deems distant ions immune to electrostatic lensing. At $3\lambda_D$, the trajectories of particles subject to electrostatic attraction are minimally modulated. At the sheath edge, such trajectories are solely dominated by thermal and bulk velocities. As one moves farther away from the charged spacecraft (i.e., greater $|y_i - r|$, and thus lower electrostatic lensing), the electrostatic focusing parameter converges to the thermal focusing parameter. For a charged spacecraft at $\phi_f, \chi_e \to \chi_t$ for $|y_i - r| \to n\lambda_D$ until $\chi_e \approx \chi_t$ at $|y_i - r| \approx 3\lambda_D$. Figure 13 shows how ions at far distances $|y_i - r|$ from the spacecraft perpendicular to the flow will tend toward purely thermal trajectories, that is, $\chi_e \to \chi_t$ as $|y_i - r| \to n\lambda_D$. Note that, for this figure, we are only considering the population of ion thermal velocities toward the wake axis. Here, y_i is the initial particle position along local vertical, and $r = 9$ cm is the satellite radius. Generally, ions injected upstream the spacecraft center within the Debye sheath (i.e., $x_i \le 0$ and $r \le |y_i| \le n\lambda_D$) are collected on the ram hemisphere and may act to enhance the net ion current collection over thermal

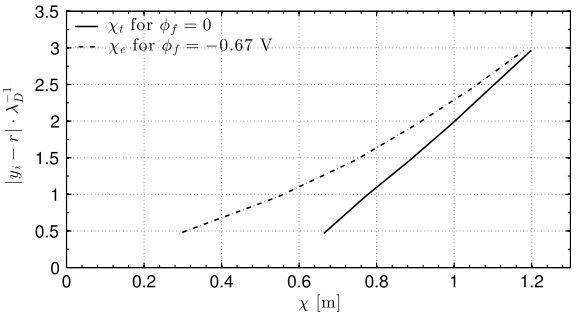

Fig. 13 Distance of particle injection from the satellite along the local vertical (y axis) and through the spacecraft center $|y_i - r|$ as a function of focusing parameter χ.

flux levels. The ion depletion in the near wake gradually becomes populated due to the electrostatic lensing of ions into the midwake and far wake.

VI. Wake Analysis

The rudimentary MATLAB simulation models a severely low ion density. Thus, the relative ion density along the wake axis is extracted by binning particles and expressing the densities as percentages of the background level set at the start of the simulation, which is an arbitrarily valued n_0. For each bin ranging 0.2 m, the density profile is normalized by the preselected background level. It is important to note that the thermal wake depicts a Mach cone, outside of which quasi neutrality holds. In actuality, ion thermal motions and energies are quasi-random according to some unknown velocity distribution function. However, the preselected ion thermal velocity vectors shown in Figs. 10 and 12 ensure a rudimentary remedy for neglecting the ion distribution function a priori. Thus, to compute the wake density due to electrostatic lensing, the background quasi-neutral plasma density starting at the location where the thermal Mach cone would have existed must be added. The net ion density along the wake axis is the superposition of normalized thermal and electrostatic wake densities.

The resulting density profile of the electrostatic wake combined with the thermal wake shows a density enhancement of 32% over background between 0.4 m $\le \chi \le$ 0.6 m. As shown in Fig. 9, the ion enhancement for a 1.5U CubeSat in the focus region is 66% over the background, which does not agree particularly well with MATLAB model results, which is for a sphere. We thus simulate a 1.5U form factor sphere with the same dimensions as the MATLAB model within SPIS. We keep all the plasma parameters the same as in Table 2. The ion density in the computational domain for spherical geometry is shown in Fig. 14. Unlike the 1.5U CubeSat of Fig. 5, the ion wake for the sphere reveals a bow shock best seen in the appropriate scaling of the color bar.

The ion density profile downstream the spherical model rendered by SPIS normalized by the background simulation density of $n_0 = 8 \times 10^9$ m^{-3} is overlaid with the normalized density profile produced by the same spacecraft geometry in MATLAB. This is illustrated in Fig. 15. The binned densities of the electrostatic wake and thermal wake are in upward and downward triangle markers, respectively. The combined electrostatic and thermal densities show an ion enhancement of 32% above background (circle markers); the normalized SPIS density along the wake axis in dash-dot agrees well. The ion focus region for the sphere in the SPIS simulation has a ≈36% density enhancement at ≈0.4 m downstream, which agrees relatively well with our independent ion-lensing MATLAB code. Thus, although our validation model does not consider particle distribution functions, ambipolar electric fields, and other Debye-scale plasma dynamics, we show that these effects are secondary to the formation of an O^+ ion focus region for CubeSats charged to $\phi_f < 0$. Our work

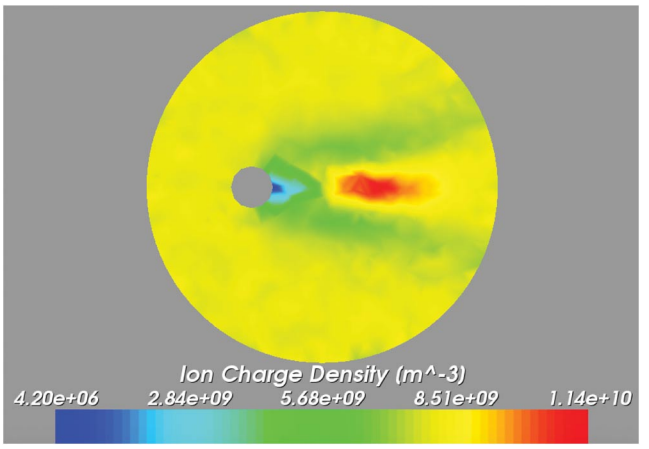

Fig. 14 Ion charge density through the principal axis along the spacecraft velocity vector for a 9 cm radius spherical satellite.

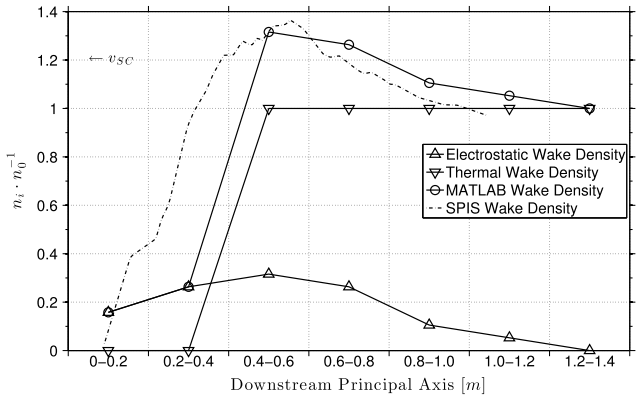

Fig. 15 Spherical spacecraft normalized O^+ wake densities for SPIS and MATLAB models.

also shows that, when the spacecraft dimensions are comparable to Debye sheath dimensions, the spacecraft geometry plays a significant role. For a low-density and cold-plasma environment, such as the one we have modeled, geometrical effects are significant; a 66% density enhancement is shown in the ion focus region for a 1.5U CubeSat as opposed to a 36% enhancement in the far wake of a similarly sized spherical spacecraft.

VII. Conclusions

The study of spacecraft–plasma interactions for CubeSats and small satellites is a growing field. Charging effects and plasma wakes of small satellites incur a departure from the thin-sheath approximation of Langmuir probe theory commonly known to describe interactions of large spacecraft in the Earth's ionosphere. Furthermore, the charging simulation package, SPIS, is gaining recognition as a robust tool in the worldwide spacecraft charging community. In mesothermal conditions of the Earth's ionosphere, the relative densities detected by wake-side and ram-side Langmuir probes are most pronounced when probes are deployed along the velocity vector, and the spin axis is perpendicular to the velocity vector. Previous studies of plasma wakes for dust grains and satellites in other environments have also revealed ion focus regions in the far wake. This paper shows that, in low-density and cold-plasma conditions, where the Debye sheath is on the same order as the CubeSat dimensions, there is a significant density enhancement in the CubeSat wake caused by ion focusing. One such condition might be in the Earth's F-region ionosphere in a low/mid latitude region inside a plasma bubble or at the topside (greater than 600 km) of the low/midlatitude ionosphere.

Using particle-in-cell simulations, this investigation cautions the experimentalists that, for small satellites, especially CubeSats, it is possible to have a plasma density enhancement above the ambient plasma density in the satellite wake. Thus, for determining the true ambient plasma density from CubeSats that deploy Langmuir probes on booms, it becomes crucial to have a correct attitude solution to determine the boom location with respect to the satellite wake. Alternatively, one can also have a properly designed length of the boom after doing a series of PIC simulations for anticipated plasma densities and spacecraft charging potentials, thus making sure that the boom tips lie outside the ion focus region. Future work includes the detailed study of geometrical dependencies on the wake structure and a refined characterization of the ion focus region.

References

[1] Barjatya, A., Swenson, C. M., and Thompson, D. C., "Invited Article: Data Analysis of the Floating Potential Measurement Unit Aboard the International Space Station," *Review of Scientific Instruments*, Vol. 80, No. 4, 2009, Paper 041301. doi:10.1063/1.3116085

[2] Barjatya, A., St-Maurice, J. P., and Swenson, C. M., "Elevated Electron Temperatures Around Twin Sporadic E Layers at Low Latitude: Observations and the Case for a Plausible Link to Currents Parallel to the Geomagnetic Field," *Journal of Geophysical Research: Space Physics*, Vol. 118, No. 11, 2013, pp. 7316–7328. doi:10.1002/2013JA018788

[3] Langmuir, I., "The Effect of Space Charge and Residual Gases on Thermionic Currents in High Vacuum," *Physical Review*, Vol. 2, No. 6, 1913, pp. 450–486. doi:10.1103/PhysRev.2.450

[4] Mott-Smith, H. M., and Langmuir, I., "The Theory of Collectors in Gaseous Discharges," *Physical Review*, Vol. 28, 1926, pp. 727–763.

[5] Lee, S., Hutputanasin, A., Toorian, A., and Lan, W., "CubeSat Design Specification Rev. 13," CubeSat Program, California State Polytechnic Univ., San Luis Obispo, CA, July 2007.

[6] Fish, C., Swenson, C., Crowley, G., Barjatya, A., Neilsen, T., Gunther, J., Azeem, I., Pilinski, M., Wilder, R., Allen, D., Anderson, M., Bingham, B., Bradford, K., Burr, S., Burt, R., Byers, B., Cook, J., Davis, K., Frazier, C., Grover, S., Hansen, G., Jensen, S., LeBaron, R., Martineau, J., Miller, J., Nelsen, J., Nelson, W., Patterson, P., Stromberg, E., Tran, J., Wassom, S., Weston, C., Whiteley, M., Young, Q., Petersen, J., Schaire, S., Davis, C., Bokaie, M., Fullmer, R., Baktur, R., Sojka, J., and Cousins, M., "Design, Development, Implementation, and on Orbit Performance of the Dynamic Ionosphere CubeSat Experiment Mission," *Space Science Reviews*, Vol. 181, Nos. 1–4, May 2014, pp. 61–120.

[7] Lai, S. T., *Fundamentals of Spacecraft Charging: Spacecraft Interactions with Space Plasmas*, Princeton Univ. Press, Princeton, NJ, 2011, p. 56.

[8] Guio, P., and Pécseli, H. L., "Phase Space Structures Generated by Absorbing Obstacles in Streaming Plasmas," *Annales Geophysicae*, Vol. 23, No. 3, March 2005, pp. 853–865. doi:10.5194/angeo-23-853-2005

[9] Kimura, S., and Nakagawa, T., "Electromagnetic Full Particle Simulation of the Electric Field Structure Around the Moon and the Lunar Wake," *Earth, Planets and Space*, Vol. 60, No. 6, July 2008, pp. 591–599. doi:10.1186/BF03353122

[10] Birdsall, C. K., and Langdon, A. B., *Plasma Physics via Computer Simulation*, Series in Plasma Physics, CRC Press, New York, NY, 2005, pp. 255–277.

[11] Miloch, W. J., Trulsen, J., and Pécseli, H. L., "Numerical Studies of Ion Focusing Behind Macroscopic Obstacles in a Supersonic Plasma Flow," *Physical Review E*, Vol. 77, May 2008, Paper 056408.

[12] Melandsø, F., and Goree, J., "Polarized Supersonic Plasma Flow Simulation for Charged Bodies Such as Dust Particles and Spacecraft," *Physical Review E*, Vol. 52, No. 5, Nov. 1995, pp. 5312–5326. doi:10.1103/PhysRevE.52.5312

[13] Maiorov, S. A., Vladimirov, S. V., and Cramer, N. F., "Plasma Kinetics Around a Dust Grain in an Ion Flow," *23rd AINSE Plasma Science and Technology Conference Held in Association with the 14th Australian Institute of Physics Conference, Conference Handbook*, Australia, 2000, p. 49. doi:10.1103/PhysRevE.63.017401

[14] Biasca, R., and Wang, J., "Ion Current Collection in Spacecraft Wakes," *Physics of Plasmas*, Vol. 2, No. 1, 1995, pp. 280–288. doi:10.1063/1.871098

[15] Keller, A. E., Gurnett, D. A., Kurth, W. S., Yuan, Y., and Bhattacharjee, A., "Lower Hybrid Waves Generated in the Wake of the Galileo Spacecraft," *Planetary and Space Science*, Vol. 45, No. 2, Feb. 1997, pp. 201–219. doi:10.1016/S0032-0633(96)00074-8

[16] Davis, V. A., Mandell, M. J., Cooke, D. L., and Enloe, C. L., "High-Voltage Interactions in Plasma Wakes: Simulation and Flight Measurements from the Charge Hazards and Wake Studies (CHAWS) Experiment," *Journal of Geophysical Research: Space Physics*, Vol. 104, No. 6, 1999, pp. 12445–12459.

[17] Schweigert, V. A., Schweigert, I. V., Melzer, A., Homann, A., and Piel, A., "Alignment and Instability of Dust Crystals in Plasmas," *Physical Review E*, Vol. 54, No. 4, Oct. 1996, pp. 4155–4166. doi:10.1103/PhysRevE.54.4155

[18] Ogilvie, K. W., Steinberg, J. T., Fitzenreiter, R. J., Owen, C. J., Lazarus, A. J., Farrell, W. M., and Torbert, R. B., "Observations of the Lunar Plasma Wake from the WIND Spacecraft on December 27, 1994," *Geophysical Research Letters*, Vol. 23, No. 10, 1996, pp. 1255–1258. doi:10.1029/96GL01069

[19] Bale, S. D., Owen, C. J., Bougeret, J. L., Goetz, K., Kellogg, P. J., Lepping, R. P., Manning, R., and Monson, S. J., "Evidence of Currents and Unstable Particle Distributions in an Extended Region Around the Lunar Plasma Wake," *Geophysical Research Letters*, Vol. 24, No. 11, 1997, pp. 1427–1430. doi:10.1029/97GL01193

[20] Farrell, W. M., Kaiser, M. L., Steinberg, J. T., and Bale, S. D., "A Simple Simulation of a Plasma Void: Applications to Wind Observations of the Lunar Wake," *Journal of Geophysical Research: Space Physics*, Vol. 103, No. 10, 1997, pp. 23,653–23,660.

[21] Samir, U., Comfort, R. H., Wright, K. H., and Stone, N. H., "Intercomparison Among Plasma Wake Models for Plasmaspheric and Ionospheric Conditions," *Planetary and Space Science*, Vol. 35, No. 12, 1987, pp. 1477–1487.
doi:10.1016/0032-0633(87)90074-2

[22] Vladimirov, S. V., Maiorov, S. A., and Cramer, N. F., "Dynamics of the Charging and Motion of a Macroparticle in a Plasma Flow," *Physical Review E*, Vol. 63, March 2001, pp. 045401-1–045401-3.

[23] Miloch, W. J., Yaroshenko, V. V., Vladimirov, S. V., Pecseli, H. L., and Trulsen, J., "Spacecraft Charging in Flowing Plasma; Numerical Simulations," *Journal of Physics: Conference Series*, Vol. 370, 2012, Paper 012004.

[24] Block, D., Carstensen, J., Ludwig, P., Miloch, W. J., Greiner, F., Piel, A., Bonitz, M., and Melzer, A., "Wake Formation and Wake Field Effects in Complex Plasmas," *Contributions to Plasma Physics*, Vol. 52, No. 10, 2012, pp. 804–812.
doi:10.1002/ctpp.201200030

[25] Lampe, M., Joyce, G., and Ganguli, G., "Structure and Dynamics of Dust in Streaming Plasma: Dust Molecules, Strings, and Crystals," *IEEE Transactions on Plasma Science*, Vol. 33, No. 1, Feb. 2005, pp. 57–69.
doi:10.1109/TPS.2004.841926

[26] Miloch, W. J., Bekkeng, T. A., and Lindem, T., "Charging and Performance of the CubeSTAR Satellite Studied by Numerical Simulations," *39th COSPAR Scientific Assembly*, Abstract C3.3-12-12, Mysore, India, July 2012, p. 1240.

[27] Mitharwal, R., "A Two-Dimensional Numerical Simulation of Plasma Wake Structure Around a CubeSat," M.S. Thesis, Utah State Univ., Logan, UT, 2011.

[28] Roussel, J.-F., Dufour, J. C., Mateo-Velez, B., Thiébault, B., Andersson, D., Rodgers, A., and Hilgers, D. P., "SPIS Multi Time Scale and Multi Physics Capabilities: Development and Application to GEO Charging and Flashover Modeling," *IEEE Transactions on Plasma Science*, Vol. 12, No. 4, 2012.

[29] Roussel, J. P., Rogier, F., Dufour, G., Mateo Velez, J.C., Forest, J., Hilgers, A., Rodgers, D., Girard, L., and Payan, D., "SPIS Open-Source Code: Methods, Capabilities, Achievements, and Prospects," *IEEE Transactions on Plasma Science*, Vol. 36, No. 5, Oct. 2008, pp. 2360–2368.
doi:10.1109/TPS.2008.2002327

[30] Sjögren, A., Eriksson, A. I., and Cully, C. M., "Simulation of Potential Measurements Around a Photoemitting Spacecraft in a Flowing Plasma," *IEEE Transactions on Plasma Science*, Vol. 40, No. 4, April 2012, pp. 1257–1261.
doi:10.1109/TPS.2012.2186616

[31] Riemann, K. U., "The Bohm Criterion and Sheath Formation," *Journal of Physics D: Applied Physics*, Vol. 24, No. 4, 1991, pp. 493–518.
doi:10.1088/0022-3727/24/4/001

[32] Barjatya, A., "Langmuir Probe Measurements in the Ionosphere," Ph.D. Dissertation, Utah State Univ., Logan, UT, May 2007.

[33] Samir, U., Stone, N. H., and Wright, K. H., "On Plasma Disturbances Caused by the Motion of the Space Shuttle and Small Satellites: A Comparison of In Situ Observations," *Journal of Geophysical Research*, Vol. 91, No. A1, Jan. 1986, pp. 277–285.
doi:10.1029/JA091iA01p00277

[34] Bellan, P. M., *Fundamentals of Plasma Physics*, Cambridge Univ. Press, New York, 2006, pp. 7–9.

E. G. Lightsey
Associate Editor